Bioorganic & Medicinal Chemistry Letters 18 (2008) 3794–3798

Contents lists available at ScienceDirect

Bioorganic & Medicinal Chemistry Letters

journal homepage: www.elsevier.com/locate/bmcl

Preliminary in vivo evaluation of a novel ^{99m}Tc-Labeled HYNIC-*cys*-annexin A5 as an apoptosis imaging agent

Humphrey Fonge [a], Marijke de Saint Hubert [b], Kathleen Vunckx [b], Dirk Rattat [a], Johan Nuyts [b], Guy Bormans [a], Yicheng Ni [c], Chris Reutelingsperger [d], Alfons Verbruggen [a,*]

[a] *Laboratory for Radiopharmacy, Faculty of Pharmaceutical Sciences, K.U. Leuven, O&N 2, Box 821, Herestraat 49, BE-3000 Leuven, Belgium*
[b] *Department of Nuclear Medicine, University Hospital Gasthuisberg Leuven, Herestraat 49, BE-3000 Leuven, Belgium*
[c] *Department of Radiology, University Hospital Gasthuisberg Leuven, Herestraat 49, BE-3000 Leuven, Belgium*
[d] *Department of Biochemistry, University Maastricht, NL-6200 Maastricht, The Netherlands*

ARTICLE INFO

Article history:
Received 10 December 2007
Revised 8 May 2008
Accepted 9 May 2008
Available online 16 May 2008

Keywords:
HYNIC-*cys*-annexin A5
Technetium-99m
Apoptosis
Imaging

ABSTRACT

A novel *cys*-annexin A5 with a single cysteine-residue at its concave side has been developed by site-directed mutagenesis to allow conjugation through thiol-chemistry without affecting its apoptotic cell binding properties and was derivatized with HYNIC in a 1:1 stoichiometry. Similar to that of the 1st generation ^{99m}Tc–HYNIC-annexin A5, the novel ^{99m}Tc–HYNIC-*cys*-annexin A5 derivative shows in normal mice mainly renal and, to a lesser extent, hepatobiliary excretion. In murine models of hepatic apoptosis there was 257% increase in hepatic uptake of ^{99m}Tc–HYNIC-*cys*-annexin A5 as compared to normal mice. Using the novel tracer agent, acute reperfused myocardial infarction in rabbits was unequivocally delineated at 7 h post-injection by μSPECT. The results indicate that the novel ^{99m}Tc–HYNIC-*cys*-annexin A5 shows similar apoptosis avidity as the 1st generation ^{99m}Tc–HYNIC-annexin A5.

© 2008 Elsevier Ltd. All rights reserved.

Cell death occurs mainly by both necrosis and apoptosis or programmed cell death.[1,2] Apoptosis is initiated by several physiological stimuli involving the activation of caspases which orchestrate a well-structured cell death program and removal of the death cells.[1,3] Apoptosis is a fundamental component of tissue development and differentiation and it also plays a significant role in a great variety of diseases. For example, during mammalian development the Müllerian duct is not needed in males, so is deleted, but it develops to the uterus in females. On the other hand, whereas excessive apoptosis is observed in diseases such as stroke, acute myocardial infarction (AMI) and progressive heart failure, insufficient apoptosis often occurs in tumor growth.[4–6] Imaging is therefore pivotal to the evaluation of these pathologies as well as assessment of response to therapeutic interventions.

Externalization of negatively charged membrane phospholipid phosphatidylserine (PS) is a major hallmark of cells undergoing apoptosis and is the sine qua non of molecular imaging of apoptosis with radiolabeled or fluorescent annexin.[7–9] Annexin A5 is a human protein of 36 kDa that binds specifically and with nanomolar affinity (K_d = 7 nM) to externalized PS in a calcium-dependent manner.[8,10] Several annexin A5 conjugates tagged with fluorophores and bifunctional chelators (BFC) have been shown to retain the affinity of native annexin A5 for PS.[11] One of the most widely used derivatives has been the hydrazinonicotinamide-annexin A5 conjugate (HYNIC-annexin A5, Fig. 1A) labeled with technetium-99m for imaging apoptosis by single-photon emission-computed tomography (SPECT). Conjugation of HYNIC to annexin for labeling with technetium-99m is usually done by targeting an amino group of one of the 21 lysine residues using *N*-succinimidyl HYNIC (*NSu-c*HYNIC), but this method is rather non-specific as any of the $-NH_2$ groups could be targeted. At the university of Maastricht, an annexin conjugate has been developed recently that permits conjugation of the HYNIC binding group in a more specific manner to the protein by incorporating a cysteine residue into annexin A5 by

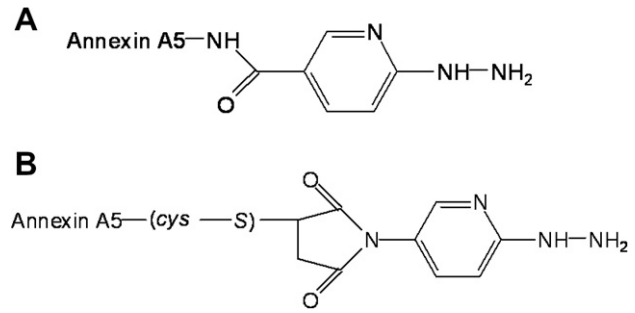

Figure 1. Structure of 1st generation HYNIC-annexin A5 (A) and novel site specific HYNIC-*cys*-annexin A5 (B).

* Corresponding author. Tel.: +32 16 33 04 46; fax: +32 16 33 04 49.
E-mail address: alfons.verbruggen@pharm.kuleuven.be (A. Verbruggen).

0960-894X/$ - see front matter © 2008 Elsevier Ltd. All rights reserved.
doi:10.1016/j.bmcl.2008.05.044

site-specific mutagenesis. Using thiol chemistry, the resulting *cys*-annexin A5 was then conjugated in a Diels–Alder reaction with 5-maleimido-2-hydraziniumpyridine hydrochloride (maleimide-HYNIC) to yield HYNIC-*cys*-annexin A5.

We herein report the labeling and preliminary in vivo evaluation of the novel site-specific ^{99m}Tc-labeled HYNIC-*cys*-annexin A5 (Fig. 1B) in normal mice and in two animal models of apoptosis, namely mice with hepatic apoptosis induced by anti-Fas monoclonal antibody (anti-Fas mAb) and in rabbits with reperfused AMI. In mice tracer uptake was studied by ex vivo biodistribution experiments and the results were compared to those of the 1st-generation ^{99m}Tc–HYNIC-annexin A5. In a rabbit model of reperfused AMI, tracer uptake was studied by μSPECT in correlation with regions of perfusion defect as assessed by positron emission tomography (μPET) using [^{13}N]NH_3 as perfusion imaging agent. Apoptosis was confirmed in situ on liver slices using the terminal deoxynucleotidyl transferase (TdT) dUTP nick end-labeling (TUNEL) assay.[12]

Annexin A5 was furnished with a single cysteine-residue at its concave side by site-directed mutagenesis to obtain *cys*-annexin A5 that allows conjugation through thiol-chemistry without affecting its apoptotic cell binding properties (submitted for publication). *Cys*-annexin A5 was derivatized with maleimide-HYNIC (Abgent, San Diego, CA, USA) to yield HYNIC-*cys*-annexin A5 with a 1:1 stoichiometry (detailed procedure to be published elsewhere). Specificity of conjugation to the thiol-functional group of the cysteine-residue was confirmed in a separate experiment by blocking the thiol-functional group of *cys*-annexin A5 with iodoacetamide and then reacting the derivative with maleimide-HYNIC under the same conditions as the derivatization of the *cys*-annexin A5 with maleimide-HYNIC. A labeling yield (labeling procedure described in detail below) of 3% and ⩾90% was obtained for acetamide-*cys*-annexin A5 and HYNIC-*cys*-annexin A5 derivatives, respectively; implying maleimide-HYNIC was specifically conjugated via the thiol-function of the cysteine residue. Labeling with technetium-99m was performed by a slight modification of a previously described procedure.[13] Briefly, in a sealed 10-mL nitrogen flushed labeling vial were consecutively added: 16 μL citrate buffer (20 mM, pH 5.2) and 0.7–1.0 GBq of $^{99m}TcO_4^-$ in 0.5 mL saline, 15 μL tricine solution (30 mg/mL in water), 12 μL $SnCl_2$ solution (10 mg $SnCl_2{\cdot}2H_2O$ in 10 mL of 0.05 M HCl) and 50–60 μg of HYNIC-*cys*-annexin A5 (in phosphate-buffered saline, PBS, pH 7.4) and the mixture was incubated at room temperature for 30 min. The reaction mixture was then purified by size exclusion liquid chromatography using a Phenomenex BioSEP SEC S3000 (300 mm × 780 mm) column (Pharmacia Biotech, Uppsala, Sweden) eluted with 0.05 M PBS at a flow rate of 1 mL/min. The purified tracer was used as such for animal studies. The 1st-generation HYNIC-annexin A5 was also labeled and purified following the same procedure. Figure 2 shows an HPLC chromatogram of the labeling mixture (retention time of ^{99m}Tc–HYNIC-*cys*-annexin A5, t_R = 11.4 min). A labeling yield ⩾90% was obtained with the above conditions. However, the presence of two radiochemical impurities eluting after radiolabeled annexin, i.e., ^{99m}Tc-tricine-citrate (t_R = 12.5 min) and [^{99m}Tc]pertechnetate (t_R = 21.5 min, Fig. 2) could not be avoided under different labeling conditions. Similar labeling yields were obtained for the 1st-generation ^{99m}Tc–HYNIC-annexin A5. The plausible structures of technetium-99m-labeled HYNIC-annexin A5 conjugates (with different co-ligands) remain to be determined, even though this has been determined for other technetium-99m-labeled HYNIC-derivatized peptides,[14] the exact co-ordination might be different for ^{99m}Tc–HYNIC-*cys*-annexin A5.

All animals received care in compliance with the principles of laboratory welfare formulated by the institutional ethical committee. Statistical significance was tested by unpaired *t*-test using GraphPad software (GraphPad, San Diego, CA, USA). $P < 0.05$ was considered statistically significant. The mice were anesthetized with isoflurane (2%) in oxygen at a flow rate of 1 L/min prior to injections. Ex vivo biodistribution studies were performed in normal NMRI mice after a tail vein injection of 300 kBq of purified ^{99m}Tc–HYNIC-*cys*-annexin A5 or ^{99m}Tc–HYNIC-annexin A5, and the animals were sacrificed at 10 min, 60 min or 4 h post injection (pi, n = 4 mice per time point). The organs were weighed and radioactivity was counted in an automated NaI(Tl) gamma counter (Wallac Wizard, Turku, Finland) and expressed as percentage of injected dose (%ID)/organ and %ID/g of organ.

Table 1 shows the biodistribution results in normal mice of novel ^{99m}Tc–HYNIC-*cys*-annexin A5 and 1st-generation ^{99m}Tc–HYNIC-annexin A5 at 10 and 60 min pi, expressed as %ID/g. The novel tracer agent ^{99m}Tc–HYNIC-*cys*-annexin A5 shows a generally similar biodistribution pattern as the 1st-generation ^{99m}Tc–HYNIC-annexin V conjugate, even though some differences can be observed. Kidney uptake was significantly different for both tracer agents at 10 min ($P = 0.009$) but was the same at 60 min ($P = 0.084$) pi. A similar significant difference was also seen in the liver uptake at 10 min ($P < 0.0001$) and 60 min ($P < 0.001$). Tait et al. also showed some striking differences in the biodistribution of different technetium-99m-labeled annexin derivatives and concluded that the protein aggregation (probably resulting from different preparation procedures) and metabolism could account for the significant difference.[15] A real conclusion can only be made after more extensive in vivo characterization. High renal cortical uptake of ^{99m}Tc–HYNIC-*cys*-annexin A5 (images not shown) has been suggested to be the result of the unique phospholipid composition of the cortex (high levels of PS) compared to papillary regions.[16]

In vivo specificity for apoptotic tissue was investigated in mice with hepatic apoptosis induced by treatment with anti-Fas mAb.[9,17] Fas receptors are abundant in hepatocytes and binding of the Fas ligand to these receptors induces apoptosis mediated by initiator and effector caspases. Ogasawara et al.[17] were the first

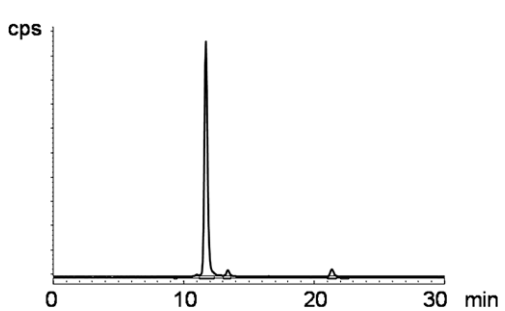

Figure 2. HPLC chromatogram of reaction mixture after labeling of HYNIC-*cys*-annexin A5 with ^{99m}Tc.

Table 1
Biodistribution of novel 'site-specific' ^{99m}Tc–HYNIC-*cys*-annexin A5 and 1st generation ^{99m}Tc–HYNIC-annexin-V in normal NMRI mice (n = 4 per time point) expressed as % of injected dose per gram of organ (%ID/g)

Organ	^{99m}Tc–HYNIC-*cys*-annexin A5 (%ID/g)		^{99m}Tc–HYNIC-annexin V (%ID/g)	
	10 min	60 min	10 min	60 min
Kidneys	39.1 ± 6.9	59.2 ± 7.8	56.9 ± 6.3	72.5 ± 8.3
Liver	11.3 ± 0.5	10.8 ± 1.0	7.1 ± 0.5	5.3 ± 0.7
Spleen + Pancreas	7.5 ± 1.0	8.3 ± 1.0	6.6 ± 4.3	3.6 ± 0.5
Lungs	16.0 ± 2.2	9.9 ± 1.1	20.5 ± 4.0	25.0 ± 3.0
Heart	3.1 ± 1.0	2.0 ± 0.1	3.1 ± 0.5	1.6 ± 0.1
Blood	6.9 ± 1.1	2.9 ± 0.2	8.7 ± 1.3	3.1 ± 0.5

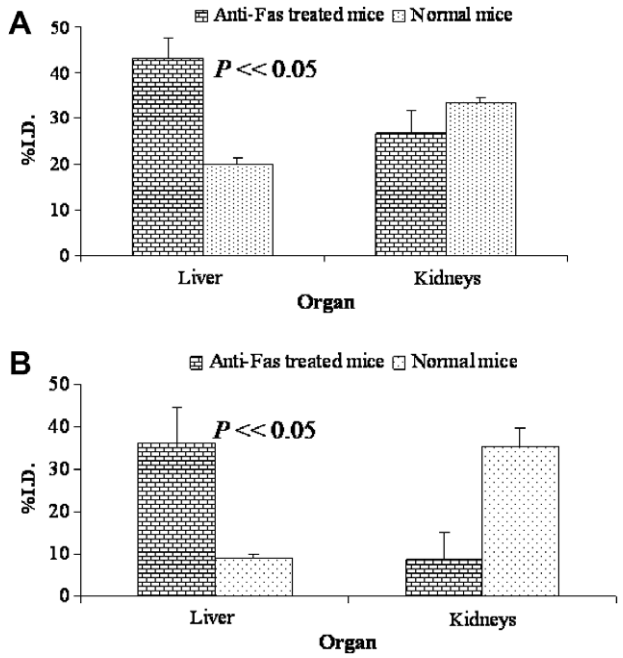

Figure 3. (A) Biodistribution of ^{99m}Tc–HYNIC-*cys*-annexin A5 and (B) 1st-generation ^{99m}Tc–HYNIC-annexin A5 (only major excretory organs are shown) in mice pre-treated with anti-Fas mAb ($n = 3$) compared to control ($n = 4$) (expressed as % injected dose, ID) at 1 h post injection. Hepatic uptake is significantly increased in apoptotic liver compared to health controls ($P << 0.05$) with a corresponding decrease in renal uptake of tracer, indicated specificity for apoptosis.

to demonstrate the lethal effect of interaction of anti-Fas mAb with its receptor. In this system only apoptotic cell death is induced. Mice (NMRI mice, body weight 25–40 g) were injected via a tail vein with purified hamster anti-Fas mAb (7–10 μg of anti-Fas mAb per mouse, Jo2, BD Pharmingen, Erembodegem, Belgium). Two hours later, pre-treated mice were injected via a tail vein with either 300 kBq of purified ^{99m}Tc–HYNIC-*cys*-annexin A5 ($n \geqslant 3$ per time point) or ^{99m}Tc–HYNIC-annexin A5 ($n \geqslant 3$ per time point) and the mice were sacrificed by decapitation under anesthesia at 1 h or 4 h pi. Figure 3 shows a comparison of uptake in major organs of pre-treated and control (without anti-Fas mAb pre-treatment) mice after injection of ^{99m}Tc–HYNIC-*cys*-annexin A5 (Fig. 3A) or ^{99m}Tc–HYNIC-annexin A5 (Fig. 3B) at 1 h pi. Liver uptake of ^{99m}Tc–HYNIC-*cys*-annexin A5 was 43.1 (± 4.7) and 19.0 (± 0.9)% ID in the anti-Fas mAb pre-treated and control groups, respectively, at 1 h pi ($P = 0.0003$). At 4 h pi there was 38.6 (± 17.8) and 10.8 (±1.4) %ID in the pretreated and controls groups, respectively ($P = 0.02$). Also kidney uptake was lower at 1 h (26.6 (±5.2) %ID in anti-Fas mAb treated as compared to 33.5 (±1.2) %ID in control mice) and at 4 h pi (18.8 (±13.8) %ID in anti-Fas mAb-treated compared to 30.7 (±1.8) %ID in control mice). Using this model of hepatic apoptosis we found a 119% and 257% increase in ^{99m}Tc–HYNIC-*cys*-annexin A5 uptake in pre-treated NMRI mice at 1 and 4 h pi, respectively. A similar high liver uptake of ^{99m}Tc–HYNIC-annexin A5 was observed in mice pre-treated with anti-Fas mAb compared to control (Fig. 3B). Tracer uptake in apoptotic liver was confirmed ex vivo by autoradiography (Cyclone Storage Phosphor System, Perkin-Elmer, Downers Grove, IL, USA) (Fig. 4A, control and apoptotic liver sections). Mean apoptotic liver to normal liver tracer uptake was 3 for both tracer agents by autoradiography. Uptake of ^{99m}Tc–HYNIC-*cys*-annexin A5 in hepatic apoptosis was similar to that of ^{99m}Tc–HYNIC-annexin A5 and the results parallel those of Blankenberg et al.[9] who also demonstrated the usefulness of ^{99m}Tc–HYNIC-annexin A5 for in vivo detection of Fas-mediated hepatic apoptosis in mice.

Apoptosis was also demonstrated in situ on 5-μm liver slices by a TUNEL assay using the ApopTag® peroxidase kit (Chemicon International, Temecula, CA, USA) according to the manufacturer's instructions. After the TUNEL assay, the sections were counterstained by immersing the slides in hematoxylin solution prior to light microscopy. Anti-Fas mAb injection led to extensive morpho-

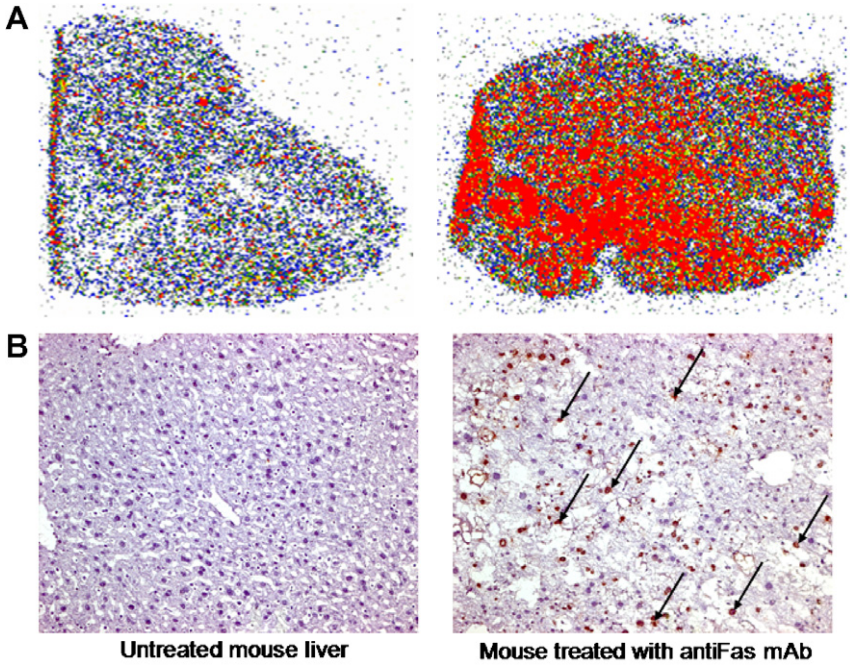

Figure 4. (A) Autoradiograms of liver of control (1st column) and anti-Fas treated mice (2nd column) after injection of ^{99m}Tc–HYNIC-*cys*-annexin A5. (B) Photomicrographs of corresponding 5-μm liver section after TUNEL staining of control (1st column) and anti-Fas-treated mice (2nd column) 3 h after antibody treatment. TUNEL-positive nuclei (brown nuclei, indicated by arrows, diaminobenzidine (DAB) was used as chromogen with hematoxylin counter stained) are diffused in treated but not in control mice and indicate apoptosis.

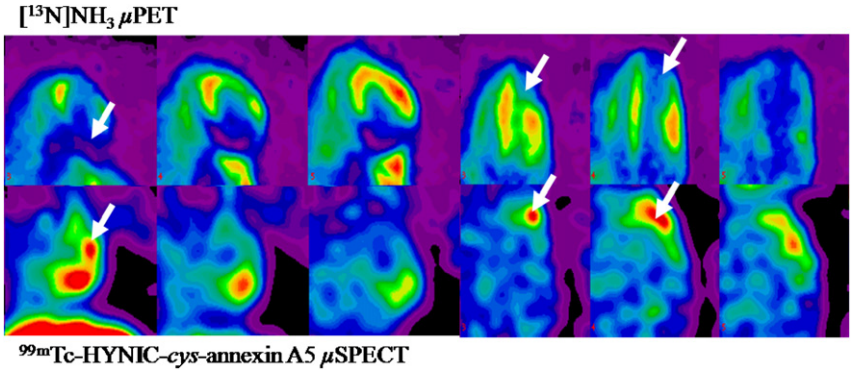

Figure 5. In vivo [^{13}N]NH_3 μPET (upper row) and ^{99m}Tc–HYNIC-*cys*-annexin A5 μSPECT (lower row) images at 7 h pi. Sets of short and long axes images are shown. Note the perfect match between the perfusion defect area (arrows) on μPET and area of high uptake (arrows) on μSPECT.

logical changes in the liver characterized by massive hemorrhage and about 30% death of animals at 3 h pi. Figure 4B shows TUNEL stained photomicrographs of liver of a control mouse liver and of a mouse pre-treated with anti-Fas mAb. TUNEL positive nuclei indicative of DNA fragmentation (characteristic hallmark of apoptosis) are seen diffused in treated but not in control mouse liver.

To further demonstrate the specificity of the novel site-specific ^{99m}Tc–HYNIC-*cys*-annexin A5 for in vivo detection of apoptosis, three rabbits (White New Zealand rabbits, 3–4 kg) with reperfused AMI were used. In this animal model, both necrosis and apoptosis are induced even though a lengthy reperfusion of the coronary artery could shift the balance towards apoptosis.[18] The detailed procedure for the animal model has been published elsewhere.[19] Anesthesia was induced and maintained with 10–20 mg/kg iv injection of sodium pentobarbital (Nembutal®). Briefly, after thoracotomy, the left circumflex coronary artery (LCx) was encircled by a snare of 2–0 suture, and occluded by sliding a piece of polyethylene tubing over the encircling snare, and both were introduced outside the chest through the incision. Reperfusion was performed after 90 min by releasing and removing the snare. Reperfusion induced arrhythmia was treated with xylocaine (0.8 mg/kg) when necessary. Temgesic® (0.3 mg/mL buprenorphine hydrochloride) was administered intramuscularly at 0.1 mg/kg for pain relief.

Two hours after infarct induction, an 8.5-min cobalt-57 transmission scan was performed prior to μPET scans. Immediately afterwards, animals were injected via an ear vein with 100 MBq of [^{13}N]NH_3 in 1.5 mL saline. Dynamic [^{13}N]NH_3 μPET imaging was performed to trace perfusion defect zones using a Siemens μPET Focus 220 LSO scanner (Knoxville, TN, USA). μPET images were acquired over a period of 30 min. The list-mode data were summed over two time frames (0–600 s and 600–1800 s). The image obtained from the second time frame was used for analysis of the zone at risk. The images were reconstructed using Fourier rebinning and a 2D ordered subsets expectation maximum (OS-EM) algorithm. Immediately afterwards, animals were injected with 106 (±23.7) MBq of ^{99m}Tc–HYNIC-*cys*-annexin A5 in 5 mL phosphate-buffered saline pH 7.4. In vivo μSPECT images were acquired at 7–9.5 h pi. μSPECT imaging experiments were performed using a dual-head gamma camera (E-cam, Siemens Medical Systems, Hoffman Estates, IL, USA), equipped with two single pinhole collimators (aperture diameter of 3 mm, Nuclear Fields International, Vortum–Mullem, The Netherlands). The μSPECT projection data were acquired in a 256 × 196 matrix with square pixels of 1.95 mm. Sixty-four projection images were measured over 360° in step-and-shoot mode with 30 s per projection angle. The detector had an intrinsic resolution of 4 mm. Reconstruction was done with the aid of the maximum likelihood ordered subsets expectation-maximum (ML-EM OS-EM) method.[20] Animals were kept under deep anesthesia with intramuscular (I.M.) injection of 1–3 mL of a mixture of 2% xylazine·HCl and 50 mg/mL ketamine.HCl (1:1, v/v) during image acquisitions. The μSPECT acquisition was immediately followed by a CT scan (Biograph16, Siemens, Knoxville, TN, USA). The animal holder contained five fiducial markers filled with ^{99m}Tc, which enabled rigid co-registration between the μSPECT and the CT images. The CT image was used for attenuation correction of the μSPECT images. In addition, it enabled co-registration between the μSPECT and the μPET images.

Myocardial tracer uptake was assembled into a polar map which was used to assess regions of myocardial infarction. All three rabbits had post-mortem evidence of infarction as assessed by staining with triphenyltetrazolium chloride (TTC, data not shown). Using ^{99m}Tc–HYNIC-*cys*-annexin A5, myocardial infarction was unequivocally delineated at 7 h pi (Fig. 5). However, images at 9 h pi show improved contrast. Regions of [^{13}N]NH_3 μPET perfusion defect match perfectly well with regions of high ^{99m}Tc–HYNIC-*cys*-annexin A5 uptake (Fig. 5). On the [^{13}N]NH_3 μPET polar map, perfusion defect was determined with a 60% threshold. The contours from this defect zone on [^{13}N]NH_3 μPET polar maps were copied to the ^{99m}Tc–HYNIC-*cys*-annexin A5 μSPECT images to determine infarct size. There was 185% (± 57.6) increase in uptake of ^{99m}Tc–HYNIC-*cys*-annexin A5 in the perfusion defect area compared to uptake in the viable myocardium at 9 h pi.

Introduction of a cysteine residue in native annexin A5 followed by derivatization with maleimide-HYNIC and labeling with ^{99m}Tc does not seem to alter the apoptosis avidity of *cys*-annexin A5 and permitted a more specific derivatization strategy to HYNIC. The study demonstrates the feasibility of in vivo detection of apoptosis in two clinically relevant settings using a novel site specific ^{99m}Tc–HYNIC-*cys*-annexin A5. In vivo binding to phosphatidylserine in cells undergoing apoptosis is retained in the novel site specific ^{99m}Tc–HYNIC-*cys*-annexin A5.

Acknowledgments

The authors thank Peter Vermaelen for the μPET imaging experiments and Tjibbe de Groot, Kristof Prinsen and Hubert Vanbilloen for practical help. This work was supported by a grant from Geconcerteerde Onderzoeksactie (GOA) of the Flemish Government, FWO-Vlaanderen Grant G. 0257.05 and in part by the EC-FP6-Project DiMI, LSHB-CT-2005-512146 and Euregional PACT Project 4-BMG-II-2 = 70.

References and notes

1. Zimmermann, K. C.; Bonzon, C.; Green, D. R. *Pharmacol. Ther.* **2001**, *92*, 57.
2. Festjens, N.; Vanden Berghe, T.; Vandenabeele, P. *Biochim. Biophys. Acta* **2006**, *1757*, 1371.

3. Thornberry, N. A. *Chem. Biol.* **1998**, *5*, R97.
4. Fliss, H.; Gattinger, D. *Circ. Res.* **1996**, *79*, 949.
5. Narula, J.; Haider, N.; Virmani, R.; DiSalvo, T. G.; Kolodgie, F. D.; Hajjar, R. J.; Schmidt, U.; Semigran, M. J.; Dec, G. W.; Khaw, B. A. *N. Engl. J. Med.* **1996**, *335*, 1182.
6. Leist, M.; Nicotera, P. *Results Probl. Cell Differ.* **1998**, *24*, 105.
7. Martin, S. J.; Reutelingsperger, C. P.; McGahon, A. J.; Rader, J. A.; van Schie, R. C.; LaFace, D. M.; Green, D. R. *J. Exp. Med.* **1995**, *182*, 1545.
8. Boersma, H. H.; Kietselaer, B. L.; Stolk, L. M.; Bennaghmouch, A.; Hofstra, L.; Narula, J.; Heidendal, G. A.; Reutelingsperger, C. P. *J. Nucl. Med.* **2005**, *46*, 2035.
9. Blankenberg, F. G.; Katsikis, P. D.; Tait, J. F.; Davis, R. E.; Naumovski, L.; Ohtsuki, K.; Kopiwoda, S.; Abrams, M. J.; Strauss, H. W. *J. Nucl. Med.* **1999**, *40*, 184.
10. Gerke, V.; Moss, S. E. *Physiol. Rev.* **2002**, *82*, 331.
11. Lahorte, C. M.; Vanderheyden, J. L.; Steinmetz, N.; Van de Wiele, C.; Dierckx, R. A.; Slegers, G. *Eur. J. Nucl. Med. Mol. Imaging* **2004**, *31*, 887.
12. Gavrieli, Y.; Sherman, Y.; Ben-Sasson, S. A. *J. Cell Biol.* **1992**, *119*, 493.
13. Verbeke, K.; Kieffer, D.; Vanderheyden, J. L.; Reutelingsperger, C.; Steinmetz, N.; Green, A.; Verbruggen, A. *Nucl. Med. Biol.* **2003**, *30*, 771.
14. King, R. C.; Surfraz, M. B.; Biagini, S. C.; Blower, P. J.; Mather, S. J. *Dalton Trans.* **2007**, 4998.
15. Tait, J. F.; Smith, C.; Blankenberg, F. G. *J. Nucl. Med.* **2005**, *46*, 807.
16. Sterin-Speziale, N.; Kahane, V. L.; Setton, C. P.; Fernandez, M. C.; Speziale, E. H. *Lipids* **1992**, *27*, 10.
17. Ogasawara, J.; Watanabe-Fukunaga, R.; Adachi, M.; Matsuzawa, A.; Kasugai, T.; Kitamura, Y.; Itoh, N.; Suda, T.; Nagata, S. *Nature* **1993**, *364*, 806.
18. Dumont, E. A.; Hofstra, L.; van Heerde, W. L.; van den Eijnde, S.; Doevendans, P. A.; DeMuinck, E.; Daemen, M. A.; Smits, J. F.; Frederik, P.; Wellens, H. J.; Daemen, M. J.; Reutelingsperger, C. P. *Circulation* **2000**, *102*, 1564.
19. Fonge, H.; Vunckx, K.; Wang, H.; Feng, Y.; Mortelmans, L.; Nuyts, J.; Bormans, G.; Verbruggen, A.; Ni, Y. *Eur. Heart J.* **2008**, *29*, 260.
20. Vanhove, C.; Defrise, M.; Franken, P. R.; Everaert, H.; Deconinck, F.; Bossuyt, A. *Eur. J. Nucl. Med.* **2000**, *27*, 140.